IOPscience iopscience.iop.org

Home Search Collections Journals About Contact us My IOPscience

Optical properties of chromium (III) in $M^{I}In(WO_4)_2$ hosts, where M^{I} = Li, Na, K, Rb

This article has been downloaded from IOPscience. Please scroll down to see the full text article.

2006 J. Phys.: Condens. Matter 18 10601

(http://iopscience.iop.org/0953-8984/18/47/007)

View the table of contents for this issue, or go to the journal homepage for more

Download details:
IP Address: 129.252.86.83
The article was downloaded on 28/05/2010 at 14:31

Please note that terms and conditions apply.

INSTITUTE OF PHYSICS PUBLISHING JOURNAL OF PHYSICS: CONDENSED MATTER

J. Phys.: Condens. Matter **18** (2006) 10601–10616 doi:10.1088/0953-8984/18/47/007

Optical properties of chromium (III) in $M^{I}In(WO_4)_2$ hosts, where M^{I} = Li, Na, K, Rb

K Hermanowicz

Institute for Low Temperature and Structure Research, Polish Academy of Sciences, PO Box 1410, 50-950 Wroclaw 2, Poland

E-mail: k.hermanowicz@int.pan.wroc.pl

Received 13 April 2006, in final form 29 September 2006
Published 13 November 2006
Online at stacks.iop.org/JPhysCM/18/10601

Abstract

Optical absorption, excitation and emission spectra have been measured for double indium tungstate crystals with the formula $M^{I}Cr_xIn_{1-x}(WO_4)_2$ (x = 0.5–2%, M^{I} = Li, Na, K and Rb) at temperatures ranging from 5 to 300 K. The broadband $^4T_2$–$^4A_2$ luminescence from low-crystal-field Cr^{3+} sites was observed in all the crystals that were studied. The local structure of the Cr^{3+} surroundings is discussed in terms of the spectroscopic results, and the crystal field parameters, Dq, B and C of the Cr^{3+} ion are derived for all the materials. The Huang–Rhys parameters, S, and breathing phonons, $\hbar\omega$, are reported. The reported data indicate a possible phase transition at about 150 K for the trigonal $RbIn(WO_4)_2$ chromium (III) doped crystals. The possible application of these crystals as laser systems is discussed.

(Some figures in this article are in colour only in the electronic version)

1. Introduction

Double molybdates and tungstates have been studied extensively for many years because of their optical, antiferroelectric and ferroelastic properties [1–7]. They are suitable as host materials for a variety of inorganic active ions, transition metal and lanthanide ions [8–12]. The transition metal ions are often applied as a structural probe due to their highly sensitive response to the changes in the surroundings because of their broad radial distribution of the outer d-electron orbital function. Among various transition metal ions, the paramagnetic chromium ion is found to be very sensitive to its chemical environment. Extensive investigations on the optical absorption, luminescence and electron spin resonance (ESR) spectroscopy of the Cr^{3+} ion in inorganic systems have been made in recent years in view of their importance in the development of tunable solid-state lasers and new luminescence materials [13–16].

The tungstates that are studied represent a very large family of crystals with the general formula $M^{I}M^{III}(M^{VI}O_4)_2$ (where M^{I} = Li, Na, K, Rb; M^{III} = Al, In, Sc, Cr, Bi, Fe, rare-earth ions, and M^{VI} = Mo, W). The aim of the present studies is the characterization of the

 © 2006 IOP Publishing Ltd Printed in the UK

spectroscopic properties of these new materials in order to obtain information about possible application of these prospective laser media. According to our knowledge, the spectroscopic properties of the alkali metal–indium double tungstates doped with Cr^{3+} ions have not yet been studied.

2. Experiment

Double tungstates were grown using the thermal method developed by Klevtsov *et al* [17] with a cooling rate of 2 K h^{-1}. Mixtures of chemically pure starting materials $M^I_2CO_3$ (M^I = Li, Na, K), In_2O_3 and WO_3 were prepared to obtain a 1:1 ratio between the $M^IIn(WO_4)_2$ double molybdate and solvent ($M^I_2W_2O_7$). Cr^{3+} doping was obtained using Cr_2O_3 as a source. The crystals obtained were of good optical quality, but of different sizes from very tiny rubidium compounds to much larger sodium crystals (2 mm × 5 mm × 8 mm). The lattice parameters of these single crystals, measured using an x-ray diffractometer (XRD), were in good agreement with data from the literature [17–24].

The experimental measurements were performed with a temperature variation between 7 and 295 K with the aid of Oxford and Janis cryostats with continuous liquid helium flow. Conventional absorption spectra were performed using a Cary 5E spectrophotometer with 5 cm^{-1} resolution. The emission and excitation spectra were recorded on a SSF-01 spectrofluorimeter. The excitation source was a 150 W xenon lamp. The system response was calibrated with a standard tungsten–halogen lamp to correct the emission spectra. Luminescence decay curves have been recorded with a Tektronix model TDS3052 digital oscilloscope following selective excitation by a continuum Surelite I optical parametric oscillator (OPO) pumped by a third harmonic of a Nd:YAG laser. The infrared (IR) spectra of the $RbIn(WO_4)_2$:Cr^{3+} crystal suspended in KBr and Nujol mull were recorded on a Biorad 575FTS spectrometer. The Raman spectra were obtained with a Bruker 100F/S spectrometer.

3. Results and discussion

3.1. Crystal structure of the hosts

$M^IIn(WO_4)_2$ crystals are attractive hosts for doping with Cr^{3+} ions, especially since they are not isostructural. This feature allows comparison of the spectroscopic properties of this ion in different environments, in spite of the fact that the structures of all hosts are derived from the structure of scheelite for potassium or wolframite for sodium and lithium [18–25].

$LiIn(WO_4)_2$ crystallizes in the monoclinic $C2/c = C^6_{2h}$ space group with $Z = 4$. The unit-cell dimensions are $a = 9.57$ Å, $b = 11.59$ Å, $c = 4.95$ Å and $\beta = 91.1°$ [18, 19]. The crystal is built up of WO^{2-}_4 ions connected to each other by means of intermolecular interactions of the $W^O{}_OW$ type, forming chains along the c-direction. The two different W···O distances are 2.36 and 2.07 Å. The $W^O{}_O W$ bridges are related to each other by a ***c*** glide plane and the double oxygen bridge symmetry is C_1. All oxygen bridges in the crystal are crystallographically equivalent and the resulting coordination of the tungstate ion is octahedral.

$NaIn(WO_4)_2$ crystallizes in monoclinic space group $P2_1/c$ ($Z = 4$) with the lattice parameters $a = 10.077$ Å, $b = 5.808$ Å, $c = 5.027$ Å, $\beta = 91.10°$ [19–23]. This structure is similar to that of the $LiIn(WO_4)_2$. Also, in this case the crystal is built up of tungstate chains. The $NaIn(WO_4)_2$ structure differs significantly, however, from that of lithium–indium double tungstate: two different kinds of oxygen bridges exist in the $NaIn(WO_4)_2$ crystal. In one type of bridge the two W···O distances are 2.09 Å, and for the other they are 2.24 Å. These differences in the crystal structures of the compounds are clearly visible in the vibrational spectra [24]. The chromium (III) ions replace the In cationic sites of the C_2 symmetry.

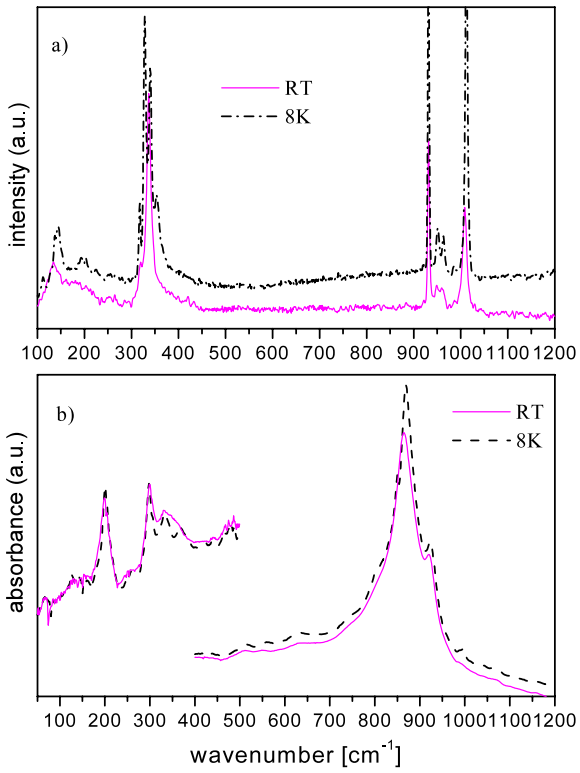

Figure 1. Polycrystalline Raman (a) and IR (b) spectra of $RbIn(WO_4)_2$:Cr^{3+} at 8 K and room temperature.

The potassium–indium double tungstate crystal may crystallize in a few different modifications, depending on the crystallization method. In ambient temperature, the monoclinic and orthorhombic phases are formed. The monoclinic $C2/c$ ($a = 10.11$ Å, $b = 5.78$ Å, $c = 14.49$ Å, $\beta = 94°$ and $Z = 1$) structure results from phase transition of the trigonal modification, which may be obtained by rapid quenching of its high-temperature phase. Slow cooling gives a low-temperature modification with orthorhombic space group $Pnam = D_{2h}^{16}$ ($Z = 4$, $a = 14.75$ Å, $b = 8.74$ Å and $c = 5.90$ Å) [25–27]. In this structure all cations are crystallographically equivalent and occupy the sites of C_s symmetry. The WO_4^{2-} ions form two sets of nonequivalent sites of C_s symmetry. The chromium (III) ions in these crystals are doped into the In^{3+} cationic sites of C_s symmetry. The In–O distances are equal to 2.102 Å for trigonal modification.

Up to now, the XRD data of the $RbIn(WO_4)_2$ crystal at ambient temperature have not been available. A suitable study for it was undertaken and these results will be published later [36]. Comparison of the measured IR and Raman spectra measured at room temperature and 8 K shows that they are very similar to those observed for trigonal and monoclinic modifications of $KIn(WO_4)_2$ samples (figure 1). IR and Raman temperature-dependent studies of $RbIn(WO_4)_2$ shows that the above phase transition takes place at about 150 K.

3.2. IR and Raman spectra

The IR and Raman spectra of all crystals studied were presented in earlier works on the vibrational spectroscopy of double molybdates and tungstates [6, 24, 28, 29]. These results

are useful in the analysis of electron–phonon coupling observed in luminescence spectra of these materials.

The internal vibrational modes of scheelite-type crystals (potassium and rubidium derivative) consist of two groups corresponding to stretching (740–990 cm^{-1}) and bending (190–491 cm^{-1}) vibrations of the tungstate anion. The number of IR and Raman components in these multiplets fits well with those predicted by the factor group analysis.

The internal vibrations of the wolframite-type $LiIn(MoO_4)_2$ and $NaIn(MoO_4)_2$ crystals reflect their structural differences compared to the scheelite-type crystals. The high degree of condensation of oxygen atoms around the W(VI) ions and the dense packing of coordination polyhedra in the unit cell lead to the octahedral coordination of the tungsten atoms. The characteristic bands corresponding to these structural fragments appear in the 500–710 cm^{-1} and 210–300 cm^{-1} regions and are assigned to the stretching and bending modes of these oxygen bond systems, respectively.

Translational modes of Li^+ ions are observed in the same wavenumber region as the bending modes, i.e. 300–500 cm^{-1}. The replacement of these ions by heavier Na^+ or K^+ leads to a frequency shift towards smaller wavenumbers. The translational modes of In^{3+} ions ($T'(In^{3+})$) are strongly coupled with $T'(WO_4^{2-})$ modes. These modes were observed as a group of strong IR and weak Raman bands in the 150–243 cm^{-1} range.

The number of $T(In^{3+})$ phonons active in the vibrational spectra reflects the symmetry of In^{3+} (and Cr^{3+}) ions in the respective unit cell. The symmetry of Cr(III) sites in CrO_6 polyhedron has important consequences for the optical spectra of these materials.

3.3. Absorption measurements

From the structure considerations it follows that three types of crystals are studied here. For the potassium derivative in the orthorhombic modification the chromium (III) ions occupy the single crystallographic site of the C_s symmetry, while for the monoclinic phase the C_2 symmetry site is occupied. The similarity of the vibrational spectra of the rubidium crystal to a trigonal $KIn(WO_4)_2$ structure follows from their IR and Raman spectra. Therefore the trigonal structure and D_{3d} site symmetry for doped chromium ions should be assumed. The sodium– and lithium–indium tungstate crystals are monoclinic and chromium ions replace the sites of C_2 symmetry.

The absorption and excitation spectra of the crystals studied, measured at 295 and 7 K, are shown in figure 2. The excitation spectra presented correlate well with respective absorption spectra of the Cr^{3+} ion. In all spectra, two characteristic broad bands are observed in the regions 430–640 nm and 590–840 nm (i.e. 15 600–23 300 and 12 000–17 000 cm^{-1}), respectively. These bands correspond to the spin-allowed $^4A_2 \rightarrow {}^4T_1$ and $^4A_2 \rightarrow {}^4T_2$ transitions of the chromium (III) ion in octahedral crystal field approximation. Due to the very large bandwidth of the $^4A_2 \rightarrow {}^4T_2$ bands and the fact that the $^4A_2 \rightarrow {}^4T_1$ band is overlapped by the low-energy wing of the band observed above 300 nm, a Gaussian fitting procedure was applied to obtain the corresponding frequency values (table 1). The shape of the $^4T_1$ and $^4T_2$ bands is different for the crystals studied (see figure 2). According to theory [30], the observed difference in relative intensities of the $^4A_2$–$^4T_2$ and $^4A_2$–$^4T_1$ bands in these crystals follows from the different strength of coupling to odd-parity distortions. It is seen especially for the sodium derivatives due to the considerably higher intensities of the $^4A_2$–$^4T_1$ broadbands compared to $^4A_2$–$^4T_2$. This follows from the fact that the coupling to T_{1u} vibrational modes is stronger than to those of T_{2u} symmetry. For the other crystals, these couplings are probably similar.

The fine structure of the $^4T_2$ absorption band is observed for all the samples, whereas for the $^4T_1$ band it can be seen for the lithium and sodium host. The spin forbidden transitions from

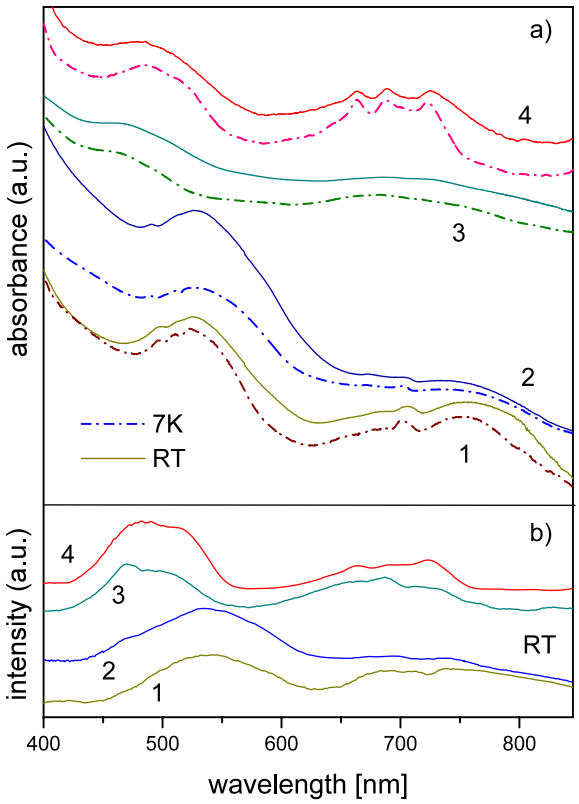

Figure 2. Absorption (a) and excitation (b) spectra of the Cr^{3+} ion in $LiIn(WO_4)_2$ (1), $NaIn(WO_4)_2$ (2), $KIn(WO_4)_2$ (3) and $RbIn(WO_4)_2$ (4) crystals at 7 K (dashed lines) and room temperature (solid lines). Due to the high similarity of the absorption spectra for the orthorhombic and monoclinic phase of the $KIn(WO_4)_2$ crystal, only the spectra measured for the orthorhombic phase are presented.

the ground state to the excited doublet terms can rarely be observed in the absorption spectra of Cr^{3+} ions. However, in some cases an interaction between the sharp intraconfigurational t_2^3 levels (^2E and $^2T_1$) and the vibronicaly broadened $^4T_2$ (t_2^2e) quasi-continuum results in Fano-type antiresonance [31–33]. Because of this, the clear and strong humps appear at 674 and 708 nm for $RbCr_{0.01}In_{0.99}(WO_4)_2$, at 676 and 710 nm for $KCr_{0.02}In_{0.98}(WO_4)_2$, at 691 and 714 nm for $NaCr_{0.01}In_{0.99}(WO_4)_2$, and at 694 and 719 nm for $LiCr_{0.01}In_{0.99}(WO_4)_2$. They are due to spin–orbit interactions with the narrow $^2T_1$ and ^2E bands. Dips of a similar nature in the $^4T_1$ shape correspond to $^4A_2$–$^2T_2$ transitions.

The optical and luminescence properties of Cr^{3+} ions are interpreted by means of a crystal-field energy diagram originating from the free-ion LS-terms of the $3d^3$ configuration. The free-ion energies are functions of inter-electron interaction Racah parameters B and C. The interaction of the 3d electrons with the octahedral lattice surroundings is characterized by the strength Dq of the octahedral crystal field. The observed optical absorption transitions allow us to evaluate the crystal-field parameters. For the octahedral symmetry approximation these parameters were calculated from the well-known expressions given by [30]. Because a clear $^4A_2 \rightarrow {}^2E$ band is not observed in both the absorption and emission spectra, the procedure of energy evaluation of the ^2E state from Fano structures was applied [34]. This procedure is illustrated in figure 4 for $LiIn(WO_4)_2$ crystal.

Table 1. Energy levels, crystal field and Racah parameters, the nephelauxetic ratio (β), the Stokes shift (SS), the Huang Rhys parameter S and ΔE (see text for explanation) obtained from the absorption and emission spectra of $MIn(WO_4)_2$:Cr^{3+} crystals, where M = Li, Na, K and Rb, at 7 and 295 K.

	$LiIn(WO_4)_2$		$NaIn(WO_4)_2$		$KIn(WO_4)_2$		$RbIn(WO_4)_2$	
	295 K	7 K	295 K	7 K	295 K	7 K	295 K	7 K
$^4T_2$ (cm^{-1})	13 680	13 770	13 320	13 330	14 480	14 430	14 050	14 500
^2E (cm^{-1})	13 890	13 930	13 980	14 010	14 140	14 230	14 130	14 150
$^2T_1$ (cm^{-1})	14 370	14 440	14 390	14 430	14 700	14 760	14 870	14 870
$^4T_1$(F) (cm^{-1})	19 150	19 200	18 650	18 680	20 920	20 270	20 745	21 520
$^2T_2$ (cm^{-1})	19 050		20 120		20 160	19 720	20 325	20 620
$^4T_1$(P) (cm^{-1})	28 940	29 210	28 650		29 140	27 320	29 040	30 150
In–O distance (Å)			2.019, 2.109, 2.231		2.102[a]		2.169[a]	
Dq (cm^{-1})	1368	1377	1332	1333	1448	1443	1405	1450
B (cm^{-1})	534	540	533	536	671	586	723	764
β	0.582	0.588	0.581	0.583	0.731	0.638	0.788	0.832
Dq/B	2.56	2.55	2.50	2.49	2.16	2.46	1.94	1.90
C (cm^{-1})	3294	3293	3329	3332	3082	3288	2979	2891
C/B	6.17	6.10	6.25	6.22	4.59	5.61	4.12	3.78
Stokes shift (SS) (cm^{-1})	4240	4525	4380	4580	2750	3050	2150	2950
S	9.33	9.86	10.92	11.56	4.37	5.26	3.48	4.65
$S\hbar\omega$	2270	2366	2240	2084	1564	1632	1554	1655
ΔE (cm^{-1})	−2330	−2422	−2850	−2970	−1035	−1325	−1050	−1125

[a] For trigonal $P\bar{3}m1$ modification above 1100 K.

According to the papers by Sturge [33] and Lempicki [34], the fitting of the ratio ($R(\omega)$) (1) between the observed absorption profile to the background given by Fano theory [35] was applied:

$$R(\omega) = 1 + \sum_i \rho^2 \frac{q_i^2 + 2q_i\varepsilon_i - 1}{1 + \varepsilon_i^2}, \tag{1}$$

where $\varepsilon_i = \frac{\omega - \omega_{ri}}{\gamma_i}$, $\hbar\omega_{ri}$ is the energy of the discrete state perturbed by the interaction with the continuum, γ_i is related to the lifetime of the same level; ρ is the fraction of continuum states $^4T_2$ interacting with sharp levels through spin–orbit coupling and q characterizes the line shape. The evaluated parameters and energy values of the ^2E state are presented in table 2. It is worth noticing that, generally, the R lines do not coincide with the $\hbar\omega_{ri}$ 'peak'. This difference follows from the coupling of the ^2E level with the continuum, and this shift is similar to the Lamb shift [31].

The energy of the electronic transitions obtained from a Gaussian procedure applied to absorption contours has been verified by comparison with those derived from Tanabe–Sugano diagrams which have been derived from the obtained crystal-field parameters of the crystals studied. An inspection of the Tanabe–Sugano diagrams and evaluated parameters shows that a distinct difference exists between the lithium and sodium derivatives from one side and potassium and rubidium derivatives from the other side. The values of the Dq/B ratio indicate a stronger crystal field in the sodium and lithium crystals. Although this high value, ∼2.5, suggests the strong crystal-field case, the calculated Tanabe–Sugano diagram proves that the energy of the $^4T_2$ and ^2E levels are comparable (figure 5). The characteristic point of the crossover is situated at values of 2.55, 2.58, 2.02 and 1.87 Dq/B for the Li, Na, K and Rb

Table 2. Parameters of the fitting of the Fano structures.

	ρ^2		q (eV)		ω_{ri} (cm^{-1})		γ (cm^{-1})	
Transition	RT	7 K	RT	7 K	RT	7 K	RT	7 K
$^4A_2$–^2E								
$LiIn(WO_4)_2$	0.037	0.055	−0.16	−0.12	13 890	13 930	350	310
$NaIn(WO_4)_2$	0.0085	0.039	0.01	0.03	13 980	14 010	230	210
$KIn(WO_4)_2$[a]	0.039	0.06	0.16	0.14	14 140	14 230	350	390
$RbIn(WO_4)_2$	0.019	0.03	0.3	0.03	14 130	14 150	330	360
$^4A_2$–$^2T_1$								
$LiIn(WO_4)_2$	0.008	0.025	−0.4	−0.015	14 370	14 440	150	150
$NaIn(WO_4)_2$	0.0019	0.009	0.61	0.61	14 390	14 430	160	150
$KIn(WO_4)_2$[a]	0.01	0.03	0.6	0.03	14 700	14 760	150	170
$RbIn(WO_4)_2$	0.009	0.004	−0.4	−0.6	14 870	14 870	350	350

[a] Orthorhombic.

derivatives, respectively. Thus in all crystal hosts the intermediate crystal-field strength is present. The value of the parameter B is a measure of the inter-electronic repulsion in the shell of d orbitals. Its inspection is useful in discussing the ionic-covalent properties of the Cr^{3+}-ligand bonding. The nephelauxetic effect takes into account the fact that the value of the inter-electronic repulsion parameter is lower for solids than for the corresponding free ion. The nephelauxetic ratio describing the delocalization of d-electrons has been evaluated using the formula $\beta = B(\text{complex})/B(\text{free ion})$, where $B_{\text{free ion}}$ is equal to 918 cm^{-1}. For the crystals studied, the lowering of β values for the lithium and sodium tungstates is significant, i.e. the β equals about 0.58. On the other hand, this lowering is much smaller for potassium and rubidium derivatives. The low values of the inter-electronic repulsion parameter B and the nephelauxetic ratio β for the Li and Na tungstates suggest that the environment of the chromium ion is more covalent in these crystals, whereas in the Rb and K hosts it is more ionic.

Lowering the temperature down to 7 K leads to some changes in the crystal-field strength for the rubidium and potassium crystals, whereas the crystal-field strength remains nearly the same for the Li and Na compounds. The absorption contour of the $^4A_2$–$^4T_1$ broadbands becomes asymmetric for potassium and rubidium, but additional dips for the lithium and sodium hosts are visible. A similar effect is seen in the spectra of highly doped (20% of chromium) sodium indium tungstate at ambient temperature (figure 3). Such behaviour probably indicates the presence of more than one active centre in the crystal matrix or considerable symmetry lowering. It is worth noting that significant similarity in the optical absorption spectra of monoclinic and orthorhombic modification of the $KIn(WO_4)_2$ hosts indicates a similar crystal-field environment of Cr^{3+} ions in these modifications.

3.4. Emission spectra

The emission measurements were made under excitation in the $^4A_2$–$^4T_1$ and $^4A_2$–$^4T_2$ absorption band. The observed emissions are characterized by a broad structureless band that corresponds to the spin-allowed $^4A_2$–$^4T_2$ transition only. This agrees with the results of the absorption studies, which revealed that the $^4T_2$ excitation state lies below the E_g level. The $^2E \rightarrow {}^4A_2$ spin-forbidden transition has not been found either at 10 K or at 300 K. The temperature dependence of the emission band shapes are presented in figure 6. The position of the emission bands for the sodium and lithium derivatives shows a small temperature dependence, resulting in the 160 cm^{-1} shift (table 3). For the potassium and rubidium

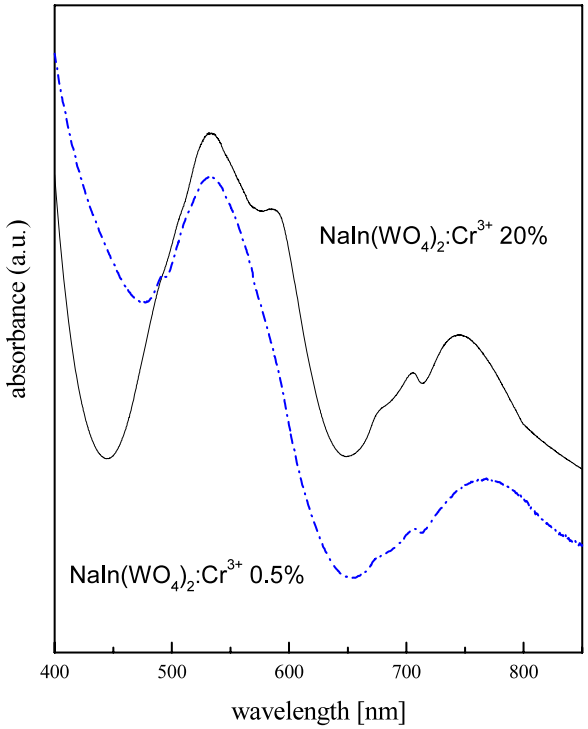

Figure 3. Comparison of the absorption spectra for different concentrations of Cr^{3+} ions in the $NaIn(WO_4)_2$ crystal.

Table 3. Maxima of the emission bands of $MIn(WO_4)_2$:Cr^{3+} crystals in (cm^{-1}), where M = Li, Na, K and Rb.

	$LiIn(WO_4)_2$	$NaIn(WO_4)_2$	$KIn(WO_4)_2$ rhombic	$KIn(WO_4)_2$ monoclinic	$RbIn(WO_4)_2$
7 K	9245	8750	11 290	11 575	11 495
300 K	9440	8940	11 730	11 900	12 005

tungstates these shifts are about 430–540 cm^{-1}, respectively, indicating the presence of several Cr^{3+} sites in $MIn(WO_4)_2$ crystals. A plot of the integrated emission intensity as a function of temperature for all crystals studied is presented in figure 7.

For the lithium, sodium and potassium orthorhombic modification the intensity decreases as the temperature increases due to a simultaneous increase of the non-radiative processes. A significantly different situation is observed for the rubidium and monoclinic modification of $KIn(WO_4)_2$ crystals. In the first stage of temperature increase, the emission intensity increases, achieving a maximum at about 150 K. Further warming to ambient temperature results in a lowering of the intensity. The temperature shift of the peak emission wavelength and the peak linewidth (FWHM) are shown in figures 7(b) and (c). For all samples, the increase in temperature from 7 K to room temperature results in an increase of the linewidth (FWHM), whereas the peak wavelengths shift to higher energies. In the plots showing the frequency values at which the maximum emission is observed as a function of temperature, some regularities are seen. For the $RbIn(WO_4)_2$ and monoclinic modification of $KIn(WO_4)_2$

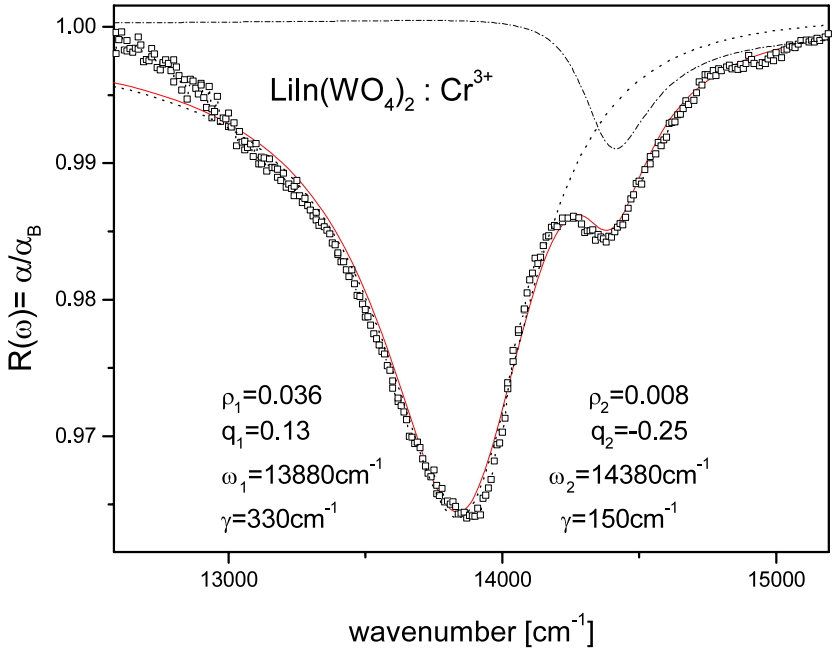

Figure 4. Fano structures obtained from the ratio between the experimental data of the absorption spectrum of the $LiIn(WO_4)_2$:Cr^{3+} and the background Gaussian shape. The broken lines present the best fit to equation (3).

crystal, the position of maximum emission changes very little in the range 295–150 K. Below this range these values decrease significantly, but for the remaining crystals the peak energy is gradually reduced over the whole 295–7 K range.

For all crystals studied, a large Stokes shift describing the shift between maxima of the absorption and emission bands is observed. This indicates that significant changes occur in the ionic arrangement around Cr^{3+} ion in the excited state. The value of this shift for the lithium and sodium crystals is quite large, being above 4000 cm^{-1}, whereas for the potassium and rubidium derivatives it is smaller, taking values in the range 2000–3000 cm^{-1}. The obtained data allow us to evaluate the Huang Rhys parameter S, a dimensionless constant characterizing the difference in the electron–lattice coupling between electronic states, defined as follows: $(SS) = (2S - 1)\hbar\omega$, where (SS) is the Stokes shift and $\hbar\omega$ is the energy of the effective phonons.

It has been shown that the shape of the broad emission bands depends strongly on the difference in electron–lattice coupling between the electronic states. The shape was approximated using the equation $I_{em} = I_0 \Sigma \exp(-S)(S^m/m!)\delta(E_{00} - mh\nu - E)$, where S is the Huang–Rhys parameter, E_{00} is the zero-phonon energy, $h\nu$ is the effective phonon energy, and m is an integer [30, 37]. The fitting procedure was started using initial values of the S, $h\nu$ and E_{00} parameters roughly estimated from the spectroscopic data. The parameters obtained from the best fit of the low-temperature emission spectra to the predicted shapes are given in table 3. For all the crystals studied, the effective energies of the phonons involved are about 210–335 cm^{-1}. In this range, some intense bands are observed in the IR and Raman spectra, corresponding to the bending modes of tungstate ions [24, 28].

The calculated values of the S parameter (see table 1) indicate strong coupling of the electron shell to the lattice in all crystals studied, particularly in the lithium and sodium

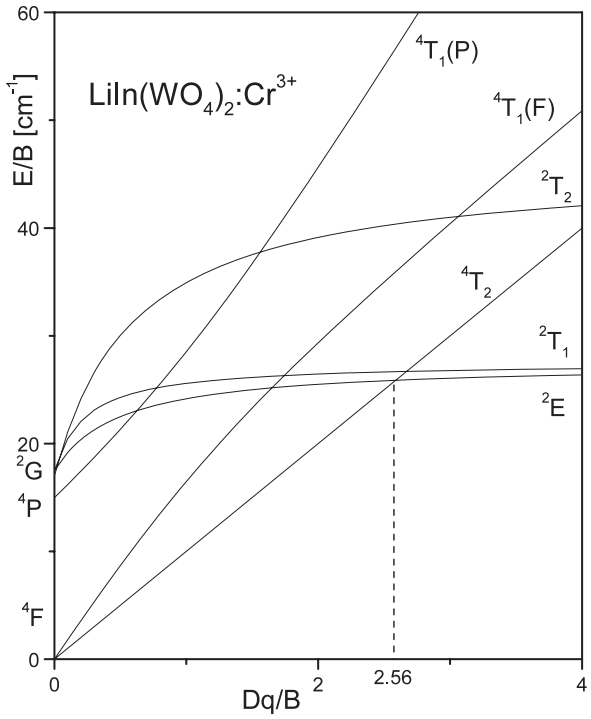

Figure 5. The Tanabe–Sugano diagram of Cr^{3+} in the lithium indium molybdate crystal obtained with the fitted parameter $C/B = 6.17$. The dotted line shows the field obtained for the $LiIn(WO_4)_2$ host.

derivatives, where the **S** values are above 9. The single configurational model (figure 8) allows us to also calculate the difference ΔE between the minima of two $^4T_2$ and ^2E parabolas. The negative value of the ΔE parameter shows (table 1) that the minimum of the $^4T_{2g}$ level is below the doublet level. As a result, the overall excitation energy after being stored in the metastable ^2E level is transferred to the $^4T_{2g}$ level, giving rise to the broad emission.

The decay profiles of the luminescence were registered only for $KIn(WO_4)_2:Cr^{3+}$ and $RbIn(WO_4)_2:Cr^{3+}$ crystals. They are nearly exponential over the whole temperature range studied. Their lifetimes decrease with increasing temperature from 390 to 13 μs for monoclinic $KIn(WO_4)_2:Cr^{3+}$ and from 288 to 11 μs for $RbIn(WO_4)_2:Cr^{3+}$ crystal (figure 9). The value of the lifetime for orthorhombic modification of the $KIn(WO_4)_2:Cr^{3+}$ crystal decreases from 40 μs at 77 K to 10 μs at room temperature. In order to explain the anomalous increase in the integral intensity of the $RbIn(WO_4)_2:Cr^{3+}$ and monoclinic $KIn(WO_4)_2:Cr^{3+}$ emissions in the 7–150 K range, the temperature-dependent measurements of the optical absorption spectra and luminescence were performed in the 300–700 nm range. The observed decrease in the integral area of the $^4A_2$–$^4T_2$ absorption band (figure 7(d)) may probably be attributed to a small reduction in the absorption coefficient with a lowering of temperature. This behaviour is distinct from the other crystals, for which the intensity of these bands remained similar or increased. In the optical spectra of the $KIn(WO_4)_2:Cr^{3+}$ and $RbIn(WO_4)_2:Cr^{3+}$ crystals in contrast to lithium, sodium and orthorhombic potassium derivatives, clearly pronounced bands below 400 nm are observed, which may be attributed to a WO_4^{2-} ligand-to-metal charge transition (LMCT) [38, 39]. Because for the tetrahedral tungstate ion a large Stokes shift

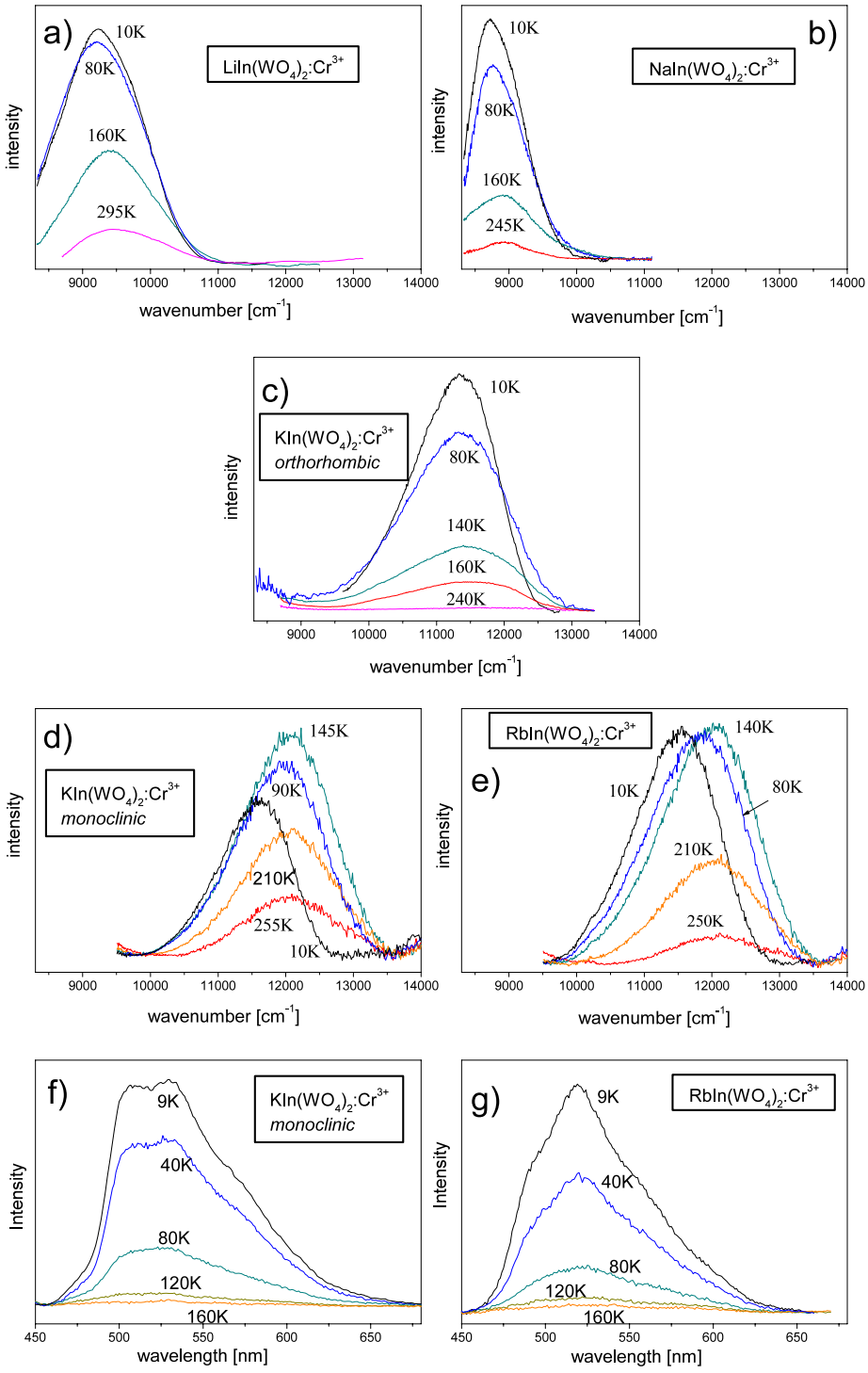

Figure 6. Emission spectra of the Cr^{3+} ion in $LiIn(WO_4)_2$, $NaIn(WO_4)_2$, $RbIn(WO_4)_2$, and orthorhombic and monoclinic $KIn(WO_4)_2$ crystals excited by a xenon lamp in the $^4A_2$–$^4T_2$ band taken at different temperatures ((a)–(e)). (f) and (g) present emission spectra of the WO_4^{2-} group for monoclinic $KIn(WO_4)_2$ and $RbIn(WO_4)_2$ crystals in the 9–160 K range.

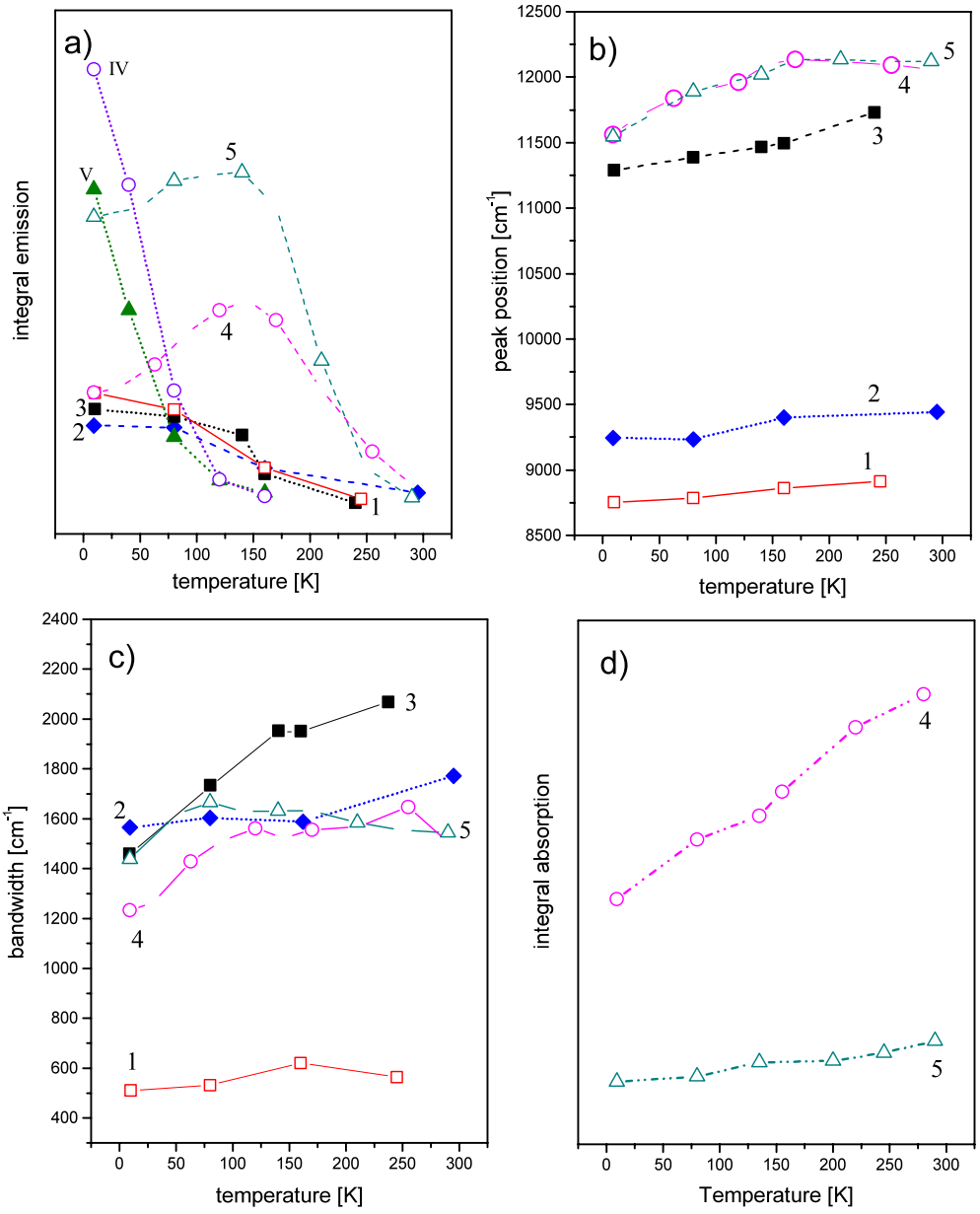

Figure 7. Temperature dependence of the integrated luminescence intensity (a), peak wavelength (b), linewidth (FWHM) centred at peak wavelength (c) of the $^4T_2$–$^4A_2$ emission, and integrated $^4T_2$–$^4A_2$ absorption band (d) of the Cr^{3+} ion in the $NaIn(WO_4)_2$ (1□), $LiIn(WO_4)_2$ (2◆), orthorhombic (3■), monoclinic (4○) $KIn(WO_4)_2$ and $RbIn(WO_4)_2$ (5△) crystals. The plots IV and V in (c) denote emissions of the WO_4^{2-} ion in the monoclinic $KIn(WO_4)_2$ and $RbIn(WO_4)_2$ crystals, respectively.

(>12 000 cm^{-1}) [40] was observed, a similar emission is expected in the visible region. From the luminescence spectra excited at about 380 nm, a strong temperature-dependent emission was found with a peak maximum observed at about 520 nm for the monoclinic

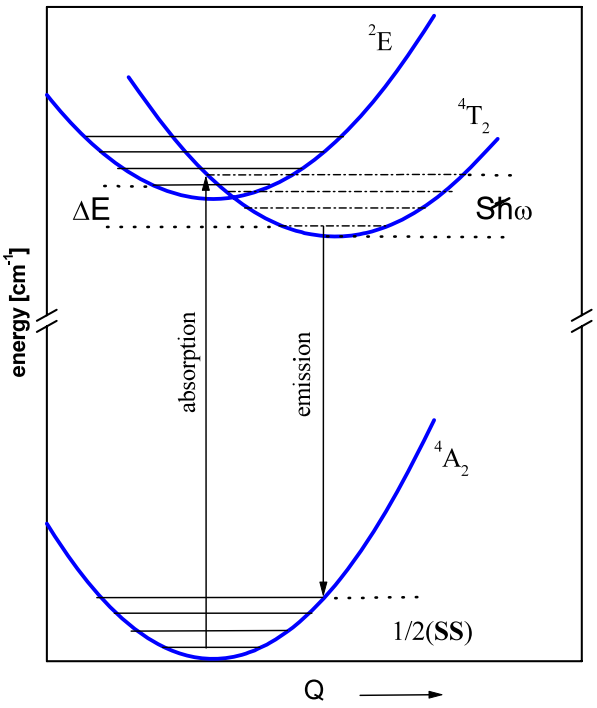

Figure 8. Single-frequency configurational coordinate model of electronic-vibrational $^4T_2$, ^2E and $^4A_2$ states.

$KIn(WO_4)_2$:Cr^{3+} and $RbIn(WO_4)_2$:Cr^{3+} crystals (figure 6). When the temperature increases from 7 to 150 K, the emission intensity drops rapidly, particularly for the potassium compound (figure 7(a)). For the other crystals studied, such strong emissions were not observed. The emissions are similar to the spectra associated with the intrinsic and extrinsic emissions that were observed for some tungstates measured previously using optical excitation [38, 40, 41]. The authors assigned these broad and structureless emission bands to the electronic transitions of the charge transfer type connected with the anion molecular complex (WO_4^{2-}). Two main types of intrinsic electronic excitations can be distinguished in tungstate crystals. One of them is the transfer of an electron from the oxygen to the tungstate ion. Another is the transfer of an electron from oxygen to the metal cation. It seems reasonable that two competitive temperature-dependent processes cause the observed maximum of the integral intensity for these samples: the non-radiative decay and emission efficiency of the tungsate group.

Possible laser applications of the materials studied can be predicted by estimation of the emission cross-section σ parameter. For $KIn(WO_4)_2$ and $RbIn(WO_4)_2$ doped Cr^{3+} crystals, the measured emission spectra could be used to calculate the effective stimulated emission cross-section of a Cr^{3+} ion from the manifold $^4T_2$–$^4A_2$ transitions by applying the Fluchtbauer–Ladenburg formula [42]: $\sigma_{em}^{peak} = \lambda_0^4/8\pi cn^2\tau_r\Delta\lambda_{eff}$, where λ_0 is the wavelength at the maximum emission, n is the refractive index of the material (approximately 2.05 for the crystals investigated), τ_r is the radiative lifetime (usually independent of the temperature), and $\Delta\lambda_{eff}$ is the effective width of the emission spectrum at room temperature defined as $\Delta\lambda_{eff} = \int I(\lambda)\,d\lambda/I_0$. In these calculations, the low-temperature lifetime values have been used as the radiative lifetimes. This assumption is justified by the low rate of non-radiative transitions

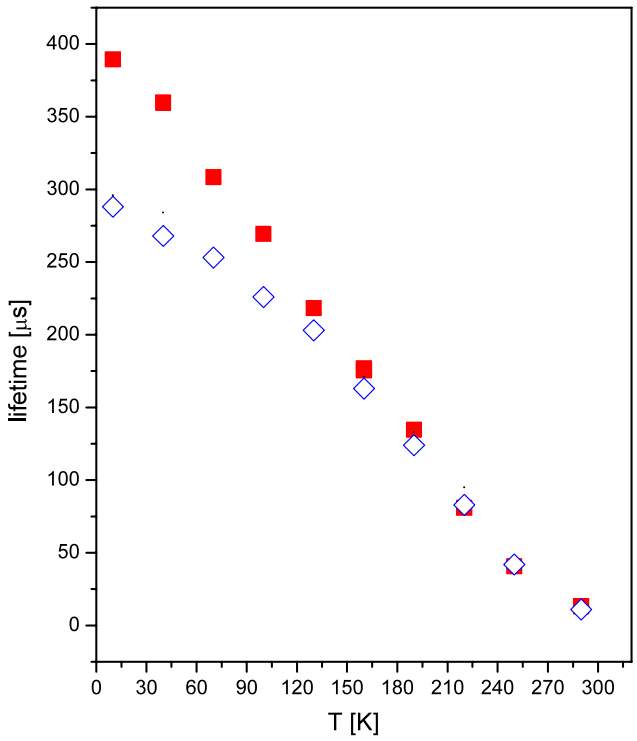

Figure 9. Emission lifetimes as a function of temperature for Cr^{3+} ion in the $RbIn(WO_4)_2:Cr^{3+}$ (◇) and monoclinic $KIn(WO_4)_2:Cr^{3+}$ (■) crystals. Lifetimes were obtained by excitation at 530 nm, and collecting at 12 250 cm^{-1}.

Table 4. Parameters obtained from the fit of the predicted shape to the emission spectra.

	E_{00} (cm^{-1})		$h\nu$ (cm^{-1})		S		$W_{nr}(0)$		σ (10^{-20} cm^{-1})	
Crystal	RT	7 K	RT	7 K	RT	7 K	RT	7 K	RT	7 K
$LiIn(WO_4)_2$	11 570	11 660	240	240	9.46	9.86	3.11×10^{-5}	8.43×10^{-5}		
$NaIn(WO_4)_2$	10 670	10 700	210	180	10.66	11.56	5.33×10^{-5}	1.72×10^{-9}		
$KIn(WO_4)_2$[a]	12 280	12 790	330	300	4.74	5.44	4.14×10^{-7}	6.58×10^{-10}	4.82	5.36
$KIn(WO_4)_2$	13 310	12 830	335	315	4.79	4.81	2.96×10^{-9}	4.05×10^{-10}	0.29	0.4
$RbIn(WO_4)_2$	12 890	12 900	335	335	4.64	4.94	1.43×10^{-8}	1.08×10^{-7}	0.51	0.48

[a] Orthorhombic.

at low temperature, calculated according to the formula $W_{nr}(0) = R_{nr}(e^{p-s}/\sqrt{2\pi p})(S/p)^p$, where R_{nf} is the non-radiative decay constant and lies in the range from 10^{12} to 10^{14} s^{-1} [43], p is the number of phonons bridging the energy gap between the excited and ground states ($p = E_{00}/h\nu$), and S is the Huang–Rhys parameter. Values of the non-radiative transition rates at low temperature, the peak wavelengths λ_0 at RT, the effective widths $\Delta\lambda$ and the values of the emission cross sections finally obtained are summarized in table 4. The emission cross-section values are somewhat larger than those for the Cr^{3+} in double indium molybdates [9], but more than a few order of magnitude smaller than observed for some high emission effective materials [44, 45].

4. Conclusions

In the present paper the optical properties of Cr^{3+}-doped alkali-indium double tungstates have been studied. From the steady-state optical absorption and luminescence measurements, it was shown that Cr^{3+} ion is incorporated in nearly octahedrally coordinated sites in all crystals studied. For these hosts the crystal-field strength, the spectroscopic Racah's parameters, the Huang–Rhys parameter and the breathing phonon frequency corresponding to the Cr^{3+} ion in the In^{3+} sites are compared in table 1. The spectroscopic data show that Cr^{3+} ions in these tungstates lie in the intermediate crystal field and, therefore, the observed emissions are characterized by broad and structureless $^4T_2$–$^4A_2$ bands. With a lowering in temperature, the second site was revealed in sodium and lithium tungstates from the absorption spectra. Among the systems studied, the $RbIn(WO_4)_2$:Cr^{3+} and the $KIn(WO_4)_2$:Cr^{3+} crystals show the highest intensity of luminescence. For the remaining crystals, the observed emission is weak at room temperature due to very effective non-radiative relaxation.

The anomalous behaviour of the integral intensity of the $RbIn(WO_4)_2$:Cr^{3+} and monoclinic $KIn(WO_4)_2$:Cr^{3+} emissions in the 7–150 K range was explained by the existence of two competing processes: non-radiative decay and the emission of the WO_4^{2-} group. The decrease in the $^4T_2$–$^4A_2$ emissions in this range is understood in terms of a large Stokes shift of the WO_4^{2-} LMCT, which can at the same time act as an energy acceptor and quencher to excited chromium states.

For all tungstates studied, a large Stokes shift and strong electron–phonon coupling have been observed. It should be noted that these crystals form a very interesting class of compounds for which the energy of the quartet levels are located so low. The phase transition from the trigonal to the monoclinic modification was revealed for the $RbIn(WO_4)_2$ crystal at about 150 K.

Acknowledgment

This work was supported by the Ministry of Science and Education under grant no 1 PO3B 078 29.

References

[1] Otko A I, Nesterenko N M and Povstyanyi L V 1978 *Phys. Status Solidi* a **46** 577
[2] Otko A I, Nesterenko N M and Zvyagin A I 1979 *Izv. Akad. Nauk SSSR, Ser. Fiz.* **43** 1675
[3] Maczka M, Hanuza J, Kao J-H and Kojima S 2003 *Phys. Rev.* B **68** 174101
[4] Zapart W 1990 *Phys. Status Solidi* a **118** 447
[5] Zapart M B and Zapart W 1993 *Phase Transit.* **43** 173
[6] Hanuza J, Mączka M, Hermanowicz K, Dereń P J, Stręk W, Folcik L and Drulis H 1999 *J. Solid State Chem.* **148** 468
[7] Maczka M, Hanuza J, Fuentes A F and Amador U 2002 *J. Raman Spectrosc.* **33** 56
[8] Macalik L, Deren P J, Hanuza J, Strek W, Demidovich A A and Kuzmin A N 1998 *J. Mol. Struct.* **450** 179
[9] Hermanowicz K, Hanuza J, Maczka M, Deren P J, Mugenski E, Drulis H, Sokolska I and Sokolnicki J 2001 *J. Phys.: Condens. Matter* **13** 5807
[10] Nikolov I, Nikolov V and Peshev P J 2003 *J. Cryst. Growth* **254** 107
[11] Neeraj S, Kijima N and Cheetham A K 2004 *Chem. Phys. Lett.* **387** 2
[12] Macalik L 2002 *J. Alloys Compounds* **341** 226
[13] Parsons-Karavassilis D, Gu Y, Ansari Z, French P M W and Taylor J R 2000 *Opt. Commun.* **181** 361
[14] De Backera A, Garreaua J C, Razdobreeva I M, Szriftgiser P, Voroshilovb I V, Lebedevb V A and Stroganova E V 2003 *Opt. Commun.* **222** 351
[15] Jun D and Deng P 2003 *Opt. Commun.* **220** 425

[16] Fromzel V A and Prasad C R 2001 *J. Phys. Chem. Solids* **62** 865
[17] Klevtsov P V, Kozeeva L P and Kharchenko L Yu 1975 *Kristallografiya* **20** 1210
[18] Klevtsov P V, Demenew A V and Klevtsova R F 1971 *Kristallografiya* **16** 520
[19] Avaeva I G, Kravchenko V B and Kobzyeva T N 1972 *Neorg. Mater.* **8** 586
[20] Karpov V N, Korotkiewich I B, Minkova M M and Sorokina O V 1973 *Zh. Neorg. Khim.* **18** 1341
[21] Kravchenko V B 1971 *Zh. Neorg. Khim.* **12** 1108
[22] Klevtsov P V and Klevtsova R F 1970 *J. Solid State Chem.* **2** 278
[23] Velikodnyi Yu A and Trunov V K 1971 *Zh. Strukt. Khim.* **12** 334
[24] Maczka M 1997 *J. Solid State Chem.* **129** 287
[25] Klevtsov P V, Klevtsova R F and Demenew A V 1972 *Kristallografiya* **17** 545
[26] Klevtsov P V and Kharchenko L Yu 1976 *Zh. Neorg. Khim.* **21** 2836
[27] Efremov V A, Trunov V K and Velikodnyi Yu A 1972 *Kristallografiya* **17** 1135
[28] Mączka M, Hanuza J, Kojima S and van der Maas J H 2001 *J. Solid State Chem.* **158** 334
[29] Maczka M 1996 *Eur. J. Solid State Inorg. Chem.* **33** 783
[30] Henderson B and Imbush G F 1989 *Optical Spectroscopy of Inorganic Solids* (Oxford: Clarendon)
[31] Fano U 1961 *Phys. Rev.* **124** 1866
[32] Fano U 1965 *Phys. Rev.* **137** A1364
[33] Sturge M D, Guggenheim H J and Pryce M H L 1970 *Phys. Rev.* B **7** 2459
[34] Lempicki A, Andrews L, Nettel S J, Collum B C and Solomon E I 1980 *Phys. Rev. Lett.* **44** 1234
[35] Fano U and Cooper J W 1965 *Phys. Rev.* A **137** 1364
[36] Maczka M 2006 in preparation
[37] Keil T H 1965 *Phys. Rev.* A **140** 601
[38] Itoh M, Alov D L and Fuijta M 2000 *J. Lumin.* **87–89** 1243
[39] Zhang Y, Holzwarth N A W and Wiliams R T 1998 *Phys. Rev.* **57** 12738
[40] Blasse G and van den Heuvel G P M 1974 *J. Lumin.* **74–78** 74
[41] Grigorjeva L, Deych R, Millers D and Chernov S 1998 *Radiat. Meas.* **29** 267
[42] Payne S A, Chase L L, Smith L K, Kway W L and Krupke W F 1992 *IEEE J. Quantum Electron.* **28** 2619
[43] Struck C W and Fonger W H 1979 *J. Lumin.* **18/19** 101
[44] Peterman K and Huber G 1984 *J. Lumin.* **31/32** 71
[45] Dong J and Deng P 2003 *J. Phys. Chem. Solids* **64** 1163